

1 Airborne transmission during short-term events: direct route  
2 over indirect route

3

4 Xiujie Li <sup>1</sup>, Zhengtao Ai <sup>2, 3\*</sup>, Jinjun Ye <sup>2, 3</sup>, Cheuk Ming Mak <sup>1</sup>, Hai Ming Wong <sup>4</sup>

5 1. *Department of Building Environment and Energy Engineering, The Hong Kong*

6 *Polytechnic University, Hong Kong, China*

7 2. *Department of Civil Engineering, Hunan University, Changsha, China*

8 3. *National Center for International Research Collaboration in Building Safety and*

9 *Environment, Hunan University, Changsha, China*

10 4. *Faculty of Dentistry, The University of Hong Kong, Hong Kong, China*

11 \*Corresponding author. Email address: zhengtaoai@hnu.edu.cn

12

13 **Abstract**

14 Numerous short-term exposure events in public spaces were reported during the

15 COVID-19 pandemic, especially during the spread of Delta and Omicron. However,

16 the currently used exposure risk assessment models and mitigation measures are mostly

17 based on the assumption of steady-state and complete-mixing conditions. The present

18 study investigates the dynamics of airborne transmission in short-term events when a

19 steady state is not reached before the end of the events. Large-eddy simulation (LES)

20 is performed to predict the airborne transmission in short-term events, and three

21 representative physical distances between two occupants are examined. Both time-

22 averaged and phase-averaged exposure indices are used to evaluate the exposure risk.

23 The results present that the exposure index in the short-term events constantly varies

24 over time, especially within the first 1/ACH (Air changes per hour) hour of exposure  
25 between occupants in close proximity, posing high uncertainty to the spatial and  
26 temporal evolutions of the risk of cross-infection. The decoupling analysis of the direct  
27 and indirect airborne transmission routes indicates that the direct airborne transmission  
28 is the predominated route in short-term events. It suggests also that the general dilution  
29 ventilation has a relatively limited efficiency in mitigating the risk of direct airborne  
30 transmission, but determines largely the occurrence time of the indirect one. Given the  
31 randomness, discreteness, localization, and high-risk characteristics of direct airborne  
32 transmission, a localized method that has a direct interference on the respiratory flows  
33 would be better than dilution ventilation for short-term events, in terms of both  
34 efficiency and cost.

35

36 **Keywords:** airborne transmission, short-term events, direct exposure, transient  
37 computational fluid dynamics (CFD), exposure risk.

38

## 39 **1. Introduction**

40 The COVID-19 pandemic, caused by the novel SARS-CoV-2 coronavirus, has swept  
41 across the world. It has led to 496 million infections including over 6 million deaths as  
42 of April 12, 2022 [1]. Owing to the detection of the positive samples of the SARS-CoV-  
43 2 virus RNA in human exhaled particles [2], it is of crucial importance in preventing  
44 airborne transmission between persons, especially at short physical distances. To a large  
45 extent, a lot of concerns have currently been raised about how to prevent the

46 transmission of SARS-CoV-2 variants and achieve economic recovery [3].

47

48 Three main transmission routes for SARS-CoV-2 have been identified: (indirect)  
49 contact, droplet transmission, and airborne transmission. Transmission through contact  
50 can be suppressed by strict surface disinfection. When the virus-carrying particles  
51 exhaled from an infected subject have settled on the skin or mucous of a susceptible  
52 subject, the droplet transmission could occur [4]. This route of transmission always  
53 takes place at a close physical distance. With regard to the airborne transmission, the  
54 respiratory micro-droplets (nuclei) suspended in the exhaled air stream could be  
55 transmitted to extended distances. The finding of 1 hour half-life of viable SARS-CoV-  
56 2 in micro-droplets [5] suggests that the unconscious infection could occur when the  
57 virus-charged particles are being inhaled. A series of precautionary measures have been  
58 proposed to prevent the probability of contact and droplet transmissions, like keeping a  
59 physical distance (such as, larger than 1-2 m), wearing a face mask, and frequent hand  
60 washing. Since airborne transmission is relatively more complicated in mechanisms  
61 and mitigation measures, the understanding of the airborne transmission routes of  
62 SARS-CoV-2 is far from sufficient.

63

64 During the COVID-19 pandemic, numerous short-term (unsteady-state) exposure  
65 events in public spaces have been reported, and the cross-transmission of the Delta  
66 variant of SARS-CoV-2 is reported to occur even in 15 seconds [6, 7]. The clustered  
67 outbreaks highlight the importance to evaluate the transient cross-transmission risks of

68 susceptible subjects and then to determine the mitigation and protection measures.  
69 However, many past studies focusing on airborne transmission were limited to the  
70 steady-state conditions by the two-equation Reynolds-averaged Navier-Stokes (RANS)  
71 turbulence models. In computational fluid dynamics (CFD) context, the numerical  
72 simulation has been widely employed to study the transmission in different scenarios  
73 like the hospitals [8, 9], office rooms [10-12], vehicles [13-15], and aircraft cabins [16,  
74 17]. The aforementioned limitation of low time-resolution studies posts a need to  
75 explore the dynamic process of the transmission of exhaled particles. The process of  
76 airborne transmission could be divided into three parts: infected individuals releasing  
77 virus-laden aerosols through the exhaled stream, the transportation of aerosols in the  
78 air, and the inhalation of aerosols by the susceptible subjects. In order to analyze the  
79 dynamics of airborne transmission, it is necessary to decouple the airborne transmission  
80 routes, namely the direct and indirect ways and to further analyze separately their  
81 characteristics. The oversimplification model with “exhalation only” for the infected  
82 subjects cannot reproduce the real situation [18-20], since the particles could only be  
83 released in the exhalation phase and the breathing flow rate is highly time-dependent.  
84 In addition, the airborne cross-transmission is considerably affected by the flow  
85 interaction in the breathing zone, including respiratory flow, ventilation flow, and  
86 thermal convective boundary layer rising from the heated human body. Overall, the  
87 study on the short-term exposure events when steady-state and complete-mixing are not  
88 reached before the end of events could provide evidence for the development of  
89 precautionary and mitigation measures.

90

91 Plenty of the exposure risk assessment models applied to the indoor environment is not  
92 suitable for short-term exposure events [21]. For example, the Wells-Riley equations  
93 have been widely employed to assess the airborne transmission risk, but the application  
94 is based on the assumption of complete mixing and thus it is limited to the steady-state  
95 conditions [22]. However, the contaminant concentration does not rise uniformly in the  
96 indoor environment, and there are many unsteady or short-term exposure events in  
97 practice when a steady state is not achieved before the end of events, such as physician  
98 consultation and short chat. To accurately evaluate the real-time exposure risk of the  
99 susceptible subject at one particular moment, it is quite critical to employ a dynamic  
100 evaluation method. Ai et al. [23] proposed the measurement and evaluation methods for  
101 short-term events on the basis of chamber experiments. However, their study is limited  
102 to several measurement points, which are not sufficient to reveal the mechanism of  
103 airborne transmission during short-term events.

104

105 Owing to the time-consuming and resource-demand characteristics of the experimental  
106 research, CFD simulations have been widely conducted to investigate the contaminant  
107 dispersion in indoor and outdoor environments. The inter-unit transmission [24, 25],  
108 and even transmission between the adjacent buildings [26, 27] have already been  
109 studied since the outbreak of SARS. In addition, the influencing factors like ventilation  
110 modes, air change rates, physical distancing, mitigation measures, and even the  
111 movement of occupants in the indoor environment have also been extensively explored

112 [28, 29].

113

114 The objective of the present study is to analyze in detail the temporal and spatial  
115 characteristics of the airborne transmission, especially in the short-term exposure  
116 events when the steady-state and complete-mixing conditions are not achieved. By  
117 capturing the interaction between the thermal convective boundary layer, the breathing  
118 respiratory flow, and ventilation flow, the direct and indirect airborne transmission  
119 would be decoupled. In addition, the short-term and steady-state flow conditions,  
120 building-up and steady-state background concentration, as well as the exposure risk  
121 with short distance and long distance would then be investigated. As a result, a better  
122 understanding of airborne transmission in the short-term exposure events could help to  
123 develop the dynamic evaluation method for risk assessment and provide the scientific  
124 basis for formulating mitigation measures.

125

## 126 **2. Mathematical model**

### 127 **2.1 LES turbulence model**

128 The turbulent flow field is composed of vortices in different scales, which play distinct  
129 roles in turbulence development. With large eddy simulation (LES), two types of  
130 motion scales would be separated by a spatial filtering operator. Since the large-scale  
131 vortices could significantly affect the average flow, having obvious anisotropy, they  
132 would be directly resolved. While the small-scale vortices, having approximate isotropy,  
133 would be modeled by a so-called sub-grid scale model. After the spatial filter operation,

134 the filtered continuity and momentum equations of the incompressible Navier–Stokes  
135 can be obtained.

136

137 The Boussinesq's hypothesis [30] is employed to calculate the sub-grid scale stress  
138 tensor  $\tau_{ij}$  by the equation  $3\tau_{ij} - \tau_{kk}\delta_{ij} = -6\mu_{SGS}\overline{S_{ij}}$ . For the incompressible flow,  
139 the term  $\tau_{kk}$  is zero, and the term  $\mu_{SGS}$  is modeled by Smagorinsky-Lilly model in  
140 the study [31]. The  $\mu_{SGS}$  is calculated by  $\mu_{SGS} = \rho L_S^2 |\overline{S}|$ , where  $|\overline{S}| \equiv \sqrt{2\overline{S_{ij}S_{ij}}}$  and  
141  $L_S$  refers to the sub-grid mixing length, calculated by  $L_S = \min(kd, C_s V^{1/3})$ . Here,  
142 the  $C_s$  is the Smagorinsky constant, empirically chosen to be 0.12. The Smagorinsky-  
143 Lilly model has been widely employed to study the flow pattern and contaminant  
144 transmission in indoor and outdoor environment [27, 32, 33].

145

## 146 **2.2 Risk assessment model**

147 The exposure risk index  $\varepsilon_s(t)$ , which indicates the relationship between ventilation  
148 and infection risk, has been extensively employed for the contaminant exposure risk  
149 evaluation in previous studies [34-36].

$$150 \quad \overline{\varepsilon_s(t)} = \frac{\overline{[C_{in}(t) - C_{supply}(t)]}}{\overline{[C_{exhaust}(t) - C_{supply}(t)]}} \quad (1)$$

151 where  $C_{supply}(t)$  and  $C_{exhaust}(t)$  refer to the contaminant concentration at the  
152 ventilation supply and the exhaust, respectively.  $C_{in}(t)$  is the inhaled concentration of  
153 the susceptible subject, and the overhead bar represents the average in the range of time  
154  $t$ .  $\overline{\varepsilon_s(t)} > 1$  indicates the worse air quality in the breathing region of the susceptible  
155 subjects than in the background or the ventilation exhaust. Considering the delayed

156 characteristics of the term  $C_{exhaust}(t)$  and the high volatility of  $C_{in}(t)$ , an improved  
 157 evaluation method proposed by Ai. et al., [23] was adopted to evaluate the dynamic  
 158 airborne transmission. Compared with the traditional exposure risk index (Eq. (1)), the  
 159 improved evaluation method makes it possible to evaluate both real-time exposure risk  
 160 of the susceptible subject at one particular moment and time-averaged exposure risk  
 161 over a given period, respectively.

$$162 \quad \varepsilon_d(t) = \frac{C_{in}(t)}{C_{exhaust-steady}} \quad (2)$$

$$163 \quad \overline{\varepsilon_d(t)} = \frac{\overline{C_{in}(t)}}{C_{exhaust-steady}} \quad (3)$$

164 where,  $\varepsilon_d(t)$  and  $\overline{\varepsilon_d(t)}$  refer to the real-time exposure index and the time-averaged  
 165 exposure index, respectively.  $C_{exhaust-steady}$  means the averaged contaminant  
 166 concentration at ventilation exhaust when reaching steady-state conditions. Phase-  
 167 averaged exposure index  $\overline{\varepsilon_{phase}(t)}$  is calculated from contaminant concentration  
 168 sampled only in the inhalation phase:

$$169 \quad \overline{\varepsilon_{phase}(t)} = \frac{\overline{C_{phase}(t)}}{C_{exhaust-steady}} \quad (4)$$

170 where,  $\overline{C_{phase}(t)}$  refers to the arithmetic mean of the concentration during the  
 171 inhalation phase. The improved evaluation method could not only avoid the delayed  
 172 building-up of concentration at the ventilation exhaust but also counteract the  
 173 intervention factors in measuring the term  $C_{in}(t)$  by normalization.

174

### 175 **3. Model description**

#### 176 **3.1 Simulation description**



177 Short-term exposure events could be divided into two types according to the status of  
178 the background pollutant concentration: the steady-state condition and the building-up  
179 condition [37]. The study focused on the last one, which refers to the infected subject  
180 having just entered the space when the event starts. The simulated scene is a room with  
181 the dimensions of 4.7 m length x 4.4 m width x 2.7 m height. As shown in Fig. 1, two  
182 computational thermal manikins (CTMs) are placed in a face-to-face position, where  
183 manikin A in red represents the infected subject and manikin B in purple refers to the  
184 susceptible one. Each manikin shares the same geometry of an average-sized woman,  
185 with a height of 1.67 m, standing on the central plane of the room. The periodic  
186 sinusoidal breathing is maintained for the manikins during the simulation. The room is  
187 in 6 air changes per hour (ACH) and the air temperature is controlled at 24 °C, which  
188 is the common room air temperature in an air-conditioned room. Mixing ventilation is  
189 adopted, with the air supply opening ( $\phi_{d1} = 0.4 \text{ m}$ ) in the middle and the exhaust  
190 diffuser (0.1 m x 0.2 m) in the corner of the ceiling. The experimental studies focusing  
191 on short-term events were conducted in a full-scale test room with three ventilation  
192 types. Two breathing thermal manikins were placed in the chamber with different  
193 standing positions and physical distances. The tracer gas concentration was monitored  
194 by the instruments, including a Fast Concentration Meter and an INNOVA Multi-gas  
195 Sampler and Monitor, to evaluate the transient exposure indices. The experimental  
196 study examined the dynamic characteristics of short-term events, and a detailed  
197 description of the apparatus and experimental procedures could be found in the previous  
198 article [23]. The boundary effect raised from the room walls in the domain would not

199 influence the human micro-environment.

200

201 In order to further reveal the mechanism of the airborne transmission, the separation of

202 the transmission routes (namely, the direct and indirect ways), is conducted. The

203 additional experiments are performed in a large space (with nearly 2870 m<sup>3</sup>) that is a

204 university canteen at off-time, where a human subject simulates an infected person and

205 the CO<sub>2</sub> concentration in the breathing zone of a thermal manikin placed in front of the

206 subject is monitored. It is believed that the exhaled CO<sub>2</sub> from a single subject is rapidly

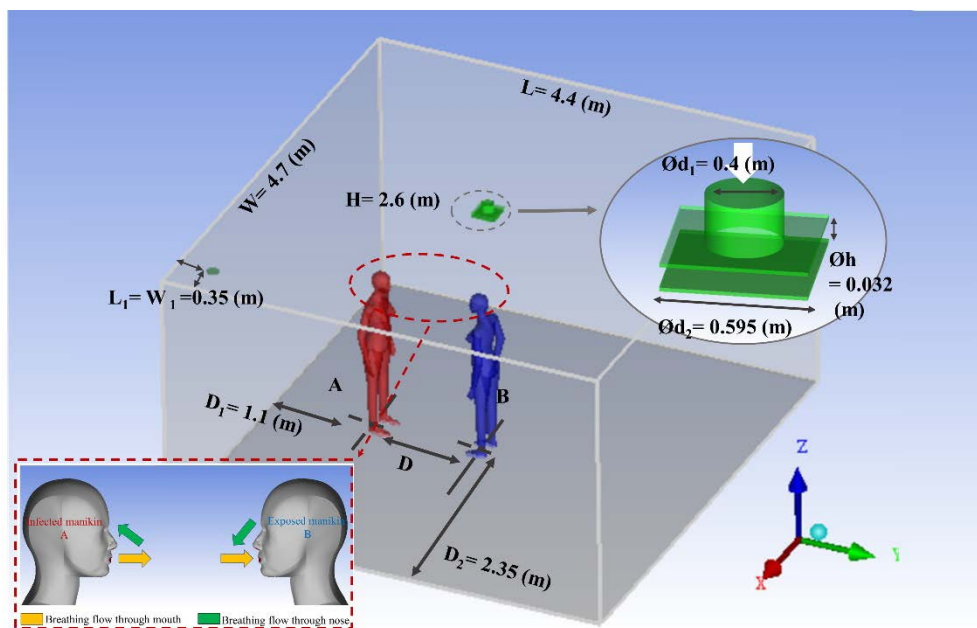
207 diluted into the indoor air of a large space and the building-up of the CO<sub>2</sub> concentration

208 in the background (referring to indirect exposure) is negligible, especially during short-

209 term events. Under this circumstance, the airborne transmission between the subject and

210 the manikin should include only direct exposure.

211



212

213 Fig.1 Simulation scenario with mixing ventilation, the physical distance (D) is

214 adjusted by moving the position of the susceptible subject (B)

215

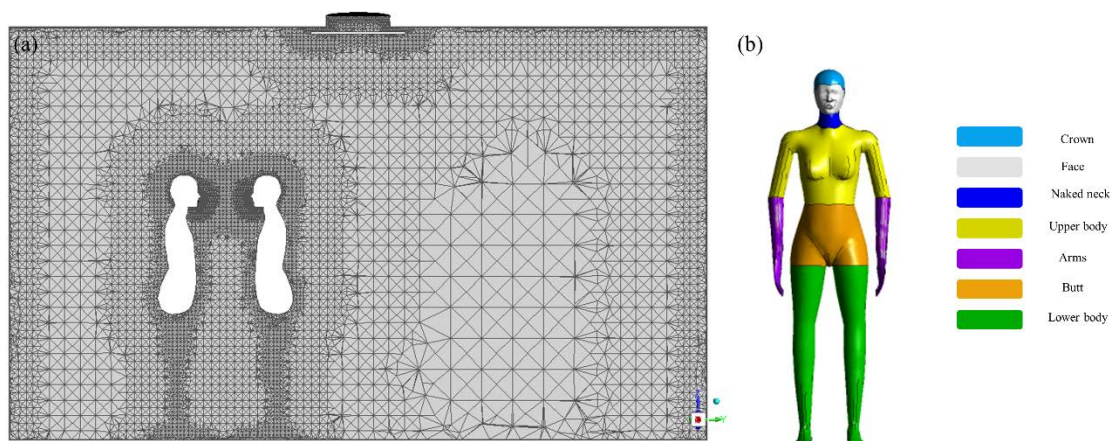
216 Since the interaction between the thermal convective boundary layer, respiratory flow,  
217 and ventilation flow largely determines the relative role of direct and indirect airborne  
218 transmission, three physical distances (D), namely 0.35 m, 1.0 m, and 1.5 m, are  
219 employed to analyze the threshold between direct and indirect transmission in short-  
220 term events. The concentration of inhaled contaminants is monitored through the  
221 sampling point in the center of the lips. In addition, the relative orientation between the  
222 two subjects is a critical factor affecting the risk of airborne transmission in a short  
223 distance. The present study considers only the face-to-face orientation, as it is the  
224 riskiest arrangement under mixing ventilation [38].

225

## 226 **3.2 Boundary conditions**

227 It has been reported that the skin temperature of the human body segments is different,  
228 and the difference might be greater than 3 °C [39]. In addition, the temperature  
229 difference among the human skin and clothing is notable owing to the insulation  
230 characteristics of the clothing [40]. To accurately reproduce the thermal convective  
231 boundary layer around the body, the CTM is divided into seven regions (as shown in  
232 Fig 2) and different skin temperatures are defined. The total heat power of each manikin  
233 is defined to be 80 W [23], where the convective heat load accounts for approximately  
234 30%. Since the present study mainly focuses on the unsteady-state flow field and  
235 contaminant distribution between two human subjects in short-term events, the

236 surrounding regions of the human body are refined by a smaller expansion ratio. The  
237 global refinement of the entire mesh is not necessary, especially for the region on the  
238 manikin's right side at the physical separation distance of 0.35 m (In Fig. 2 (a)). While  
239 the physical distance increases to 1.0 m and 1.5 m, the aforementioned region in a high  
240 aspect ratio will disappear.



241  
242 Fig. 2 (a) the grid arrangement in the domain; (b) the division of the computational  
243 thermal manikin for segmental skin variation

244  
245 As for the breathing mode, the infected subject is inhaled by the nose and exhaled by  
246 the mouth, while the susceptible subject is inhaled by the mouth and exhaled by the  
247 nose. The above combination has been recognized as the worst breathing condition in  
248 terms of the risk of cross-transmission [18]. The cross-sectional area of each nostril is  
249  $38.5 \text{ mm}^2$ , and that of the mouth is  $158 \text{ mm}^2$  [41]. The two jets from the nostrils are  
250 inclined  $45^\circ$  downwards from the horizontal plane and  $30^\circ$  from each other [42], and  
251 the flow from the mouth is roughly horizontal. The pulmonary ventilation rate and  
252 respiratory rates are  $6.0 \text{ L/min}$  and  $10 \text{ times/min}$ , respectively. Respiratory activities of

253 the CTMs follow the sinusoidal function and each breathing cycle is composed of  
254 inhalation (2.5 seconds), exhalation (2.5 seconds), and break (1.0 seconds) [43, 44].  
255 The mass fraction of tracer gas ( $N_2O$ ) in the exhalation air of the infected subject is  
256 0.027 [45]. The user-defined function is employed to add the respiratory equations to  
257 the mouth and nostrils boundary condition, and therefore the breathing speed change  
258 would follow the sinusoidal curve, as shown in Fig. 3. The other boundary conditions  
259 are presented in Table 1.

260

261 The Pressure Implicit with Split Operator algorithm (PISO) is adopted to solve the flow  
262 field. As for the space discretization of the energy, momentum, and density, the second-  
263 order upwind scheme is employed. The transient formulation is resolved by the second-  
264 order implicit method. The time step is defined as 0.04 s. Large-eddy turnover time is  
265 the characteristic timescale defined as the largest scale of the computational domain ( $w$ )  
266 divided by the friction velocity ( $v_0$ ). In this study, the  $w = 4.7 m$ , and estimated  $v_0$   
267 could be obtained by dividing the ventilation flow rate by a half section of the domain.  
268 The convergence test would be performed by evaluating the variability of the time-  
269 averaged values with a 5 eddy turnover time, and 5 eddy turnover time has been larger  
270 than that proposed by Villafruela et al. [18].

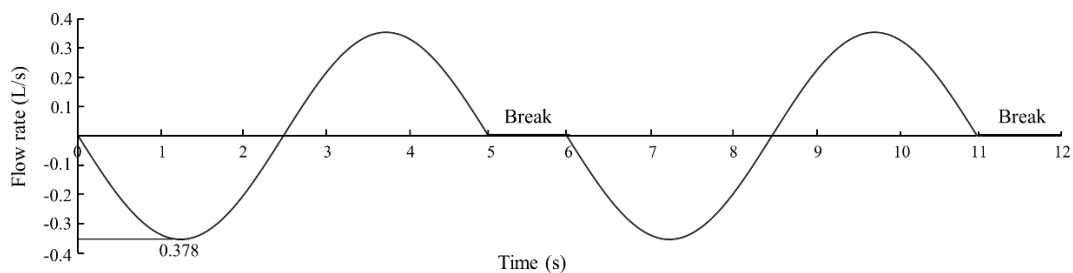
271

272

Table 1 the setting of numerical boundary conditions

Boundary	Setting
Mouth area	158 mm <sup>2</sup>

Nostril area	77 mm <sup>2</sup>
Breathing rate	6.0 L/min
Breathing frequency	10 times/min
Breathing velocity	User-defined function
Air inlet	V=0.74 m/s
Air outlet	Pressure outlet
Room wall	Adiabatic
Human body	Different temperature
Mass fraction of tracer gas	0.027



273

274 Fig. 3 The evaluation of breathing flow rate of the CTMs that is implemented by user-  
275 defined function

276

### 277 3.3 Grid independence test and model validation

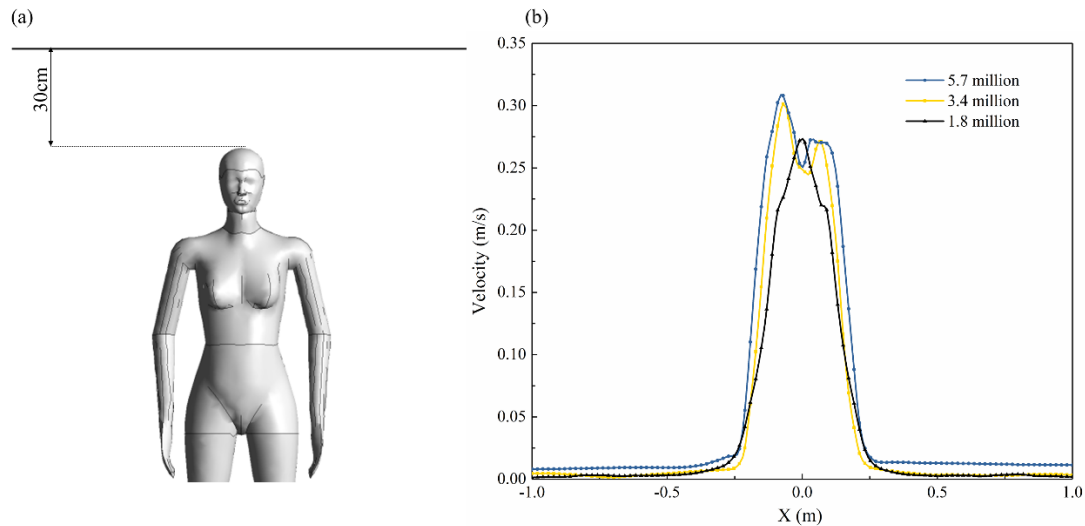
278 To save the computational cost and guarantee the reliability of the simulation, the grid  
279 independence test is carried out before the simulation. Owing to the complex human  
280 body geometry, tetrahedral cells have been employed to accurately fit the realistic  
281 geometry. The finest cell size is kept around 0.0008 m at each manikin's mouth and  
282 nose, and the cell of the face gradually expands up to 10 times. The maximum cell size

283 of the face is maintained within 10 times of that at the mouth [46], and the maximum  
284 cell size of the body was maintained within 4 times of the maximum cell size of the  
285 face. As a result, each CTM has approximately 80000 triangles on its surface. At the  
286 same time, five layers of prismatic cells are generated by extruding the surface triangles  
287 away from the surface to ensure that the  $y^+$  is less than 1. In this way, the grid could  
288 ensure a good resolution in the boundary layer, providing the best support for LES.

289

290 Three sets of grid distribution are tested, including fine: 5.7 million, medium: 3.4  
291 million, and coarse: 1.8 million. The velocity results along the sampling line above the  
292 manikin (see Fig. 4 (a)) are employed to examine the grid independence, and the  
293 comparison of the results given by using the three grids is shown in Fig. 4 (b). The  
294 medium and fine grids provide quite similar results, and the difference in the  
295 dimensionless velocity given by the fine and medium grids is 3.7%. In addition, the  
296 medium grid with 3.4 million cells is able to refine the surrounding regions of human  
297 bodies. The skewness of more than 99.6% of the cells is less than 0.91 [47]. Therefore,  
298 the simulations are conducted with the medium grid to save computational time.

299



300

301 Fig. 4 Grid independence test (a) the location of sampling line; (b) the comparison

302 of the velocity results

303

304 The model validation based on the surrounding flow field around the CTM has been  
 305 performed. The simulation results are compared to the particle image velocimetry (PIV)

306 measurements at the ambient air temperature of 20 °C [40]. In addition to the LES

307 model, the RNG  $k - \varepsilon$  model is also employed to do the comparison, by keeping the

308 same settings with the LES model. Flow speeds at fifteen points at different heights in

309 front of the thermal manikin are measured. The simulation results from 61 s to 65 s at

310 each point are averaged and compared with the experimental data, as presented in Fig.

311 5. In general, the simulation results agree well with the experimental data at most points,

312 though relatively large discrepancies occur in the region in front of the face. The reasons

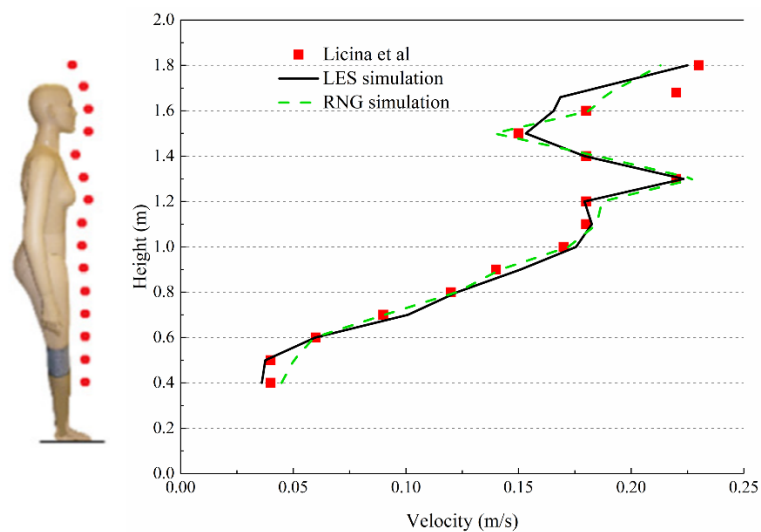
313 could be firstly the imperfection of the numerical model and settings and secondly the

314 limitation of the measurements in terms of the inaccurate determination of the sampling

315 location and the intrusion of the sampling tube. In comparison with the LES model, the



316 unsteady RANS approach just models the turbulence and resolves only unsteady mean  
 317 flow structures [48]. Since the present study focuses on short-term events, the  
 318 contaminant fluctuation depends not only on the turbulence intensity near the facial  
 319 region, but it could also be affected by the turbulent energy distribution among the  
 320 eddies of different sizes. Therefore, it is of critical importance to employ the LES  
 321 turbulence model to resolve the eddies of the turbulence itself.



322  
 323 Fig. 5 Comparison of velocity results given by the simulation and the experiment

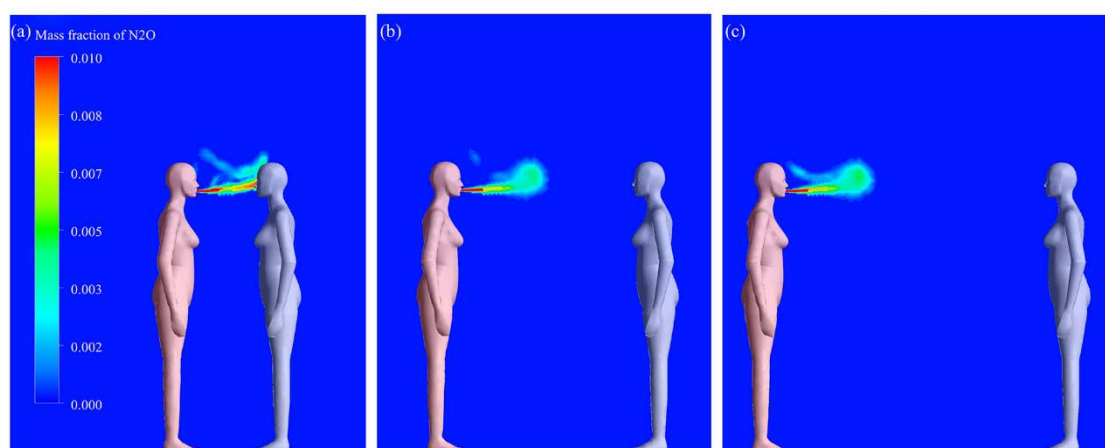
324

## 325 4. Results and analysis

### 326 4.1 Interaction of flows in breathing zone

327 Fig. 6. presents the contours of the mass fraction of  $N_2O$  on the central plane of the  
 328 chamber. In the physical distance of 0.35 m, as shown in Fig. 6 (a), the high contaminant  
 329 concentration is observed in the breathing zone of the susceptible subject. Owing to the  
 330 high momentum of respiratory flow, the exhaled aerosols surrogated by tracer gas could  
 331 penetrate the thermal convective boundary layer and the exhaled flow of the susceptible  
 332 subject at this close physical distance. In addition, the nose exhalation (namely, the

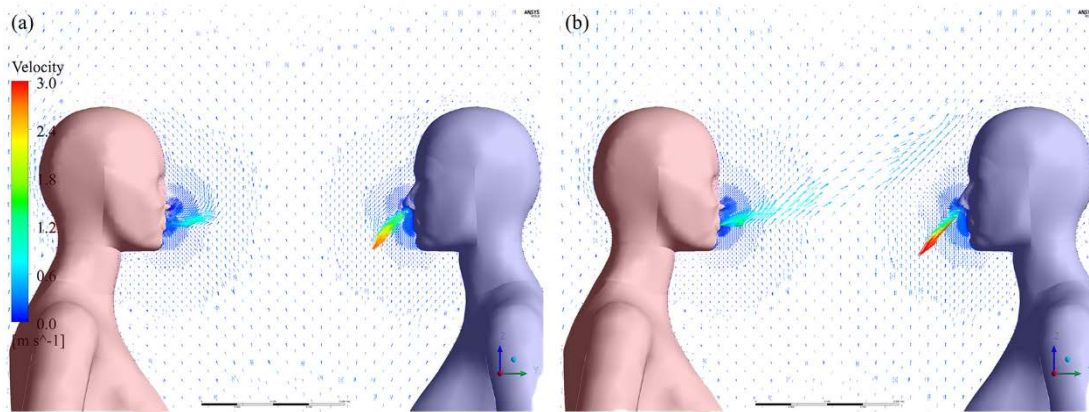
333 susceptible subject) is less effective in removing the contaminants in the breathing zone.  
334 However, at the physical distance of 1.0 m and 1.5 m (Fig. 6 b and c), it is rather difficult  
335 for the exhaled flows to penetrate the thermal convective boundary layer. Exhaled  
336 contaminants would move upward and cross over the susceptible subject under the  
337 effect of thermal convective boundary layer, diluting into the indoor air. In all distances,  
338 the phenomenon of backward movement of exhaled flows to the upper region of the  
339 infected subject is observed, thus increasing the contaminant concentration close to the  
340 infected subject's face. This phenomenon is also reported in a previous study based on  
341 dynamic breathing condition [46]. In theory, direct airborne transmission refers to the  
342 direct inhalation of exhaled contaminant owing to the close contact, and indirect  
343 transmission represents sharing of the background concentration. Given that the  
344 exposure concentration decreases considerably when the distance increases from 0.35  
345 m to 1.0 or 1.5 m, the direct and indirect airborne transmission could be identified in  
346 the range from 1.0 to 1.5 m, which is consistent with other studies [49, 50].



347  
348 Fig. 6 The mass fraction of  $N_2O$  on the central plane of the chamber with different  
349 physical distances: a)  $D = 0.35$  m; b)  $D = 1.0$  m; c)  $D = 1.5$  m. CTM in red represents  
350 the infected subject and CTM in purple refers to the susceptible one.

351

352 Further analysis of the transient interaction of the ventilation flow, respiratory flow, and  
353 thermal convective boundary layer around the two CTMs is made. Fig. 7 presents the  
354 velocity vector fields at two different moments in the exhalation process during the 20<sup>th</sup>  
355 calculated breathing cycle. When the flow is exhaled from the mouth of the infected  
356 subject, it moves upward at a distance of 0.075 m away from the mouth. A large-scale  
357 vortex is formed on the top side of the mushroom-shaped flow. The mouth breathing  
358 flow is strongly affected by the thermal convective boundary layer, which is  
359 demonstrated in some previous experiments and simulations [51, 52]. In comparison,  
360 the influence of the thermal convective boundary layer on the flow jets from the nostrils  
361 is insignificant, as the exhaled flow from nostrils has a relatively high speed and a  
362 certain downward inclination angle. When losing the initial momentum, the flow jets  
363 exhaled from the nostrils would be dragged upwards under the effect of buoyancy.  
364 However, the existence of a high-speed exhaled flow from the nostrils of the susceptible  
365 subjects could promote the generation of a low-pressure recirculation in front of the  
366 face, which might further leads to the entrainment of surrounding air (including that  
367 exhaled by the infected subject) into the breathing zone [21]. At a later stage of the  
368 exhalation process (see Fig. 7b), the exhaled flow could directly penetrate into the  
369 breathing zone of the susceptible subject and causes risk.



370

371 Fig. 7 Transient velocity vector field in the breathing zone of the two manikins at the  
 372 physical distance of 0.35 m (a) 0.5 s after the start of the exhalation phase; (b) 1.5 s  
 373 after the start of the exhalation phase. CTM in red represents the infected subject and  
 374 CTM in purple refers to the susceptible one.

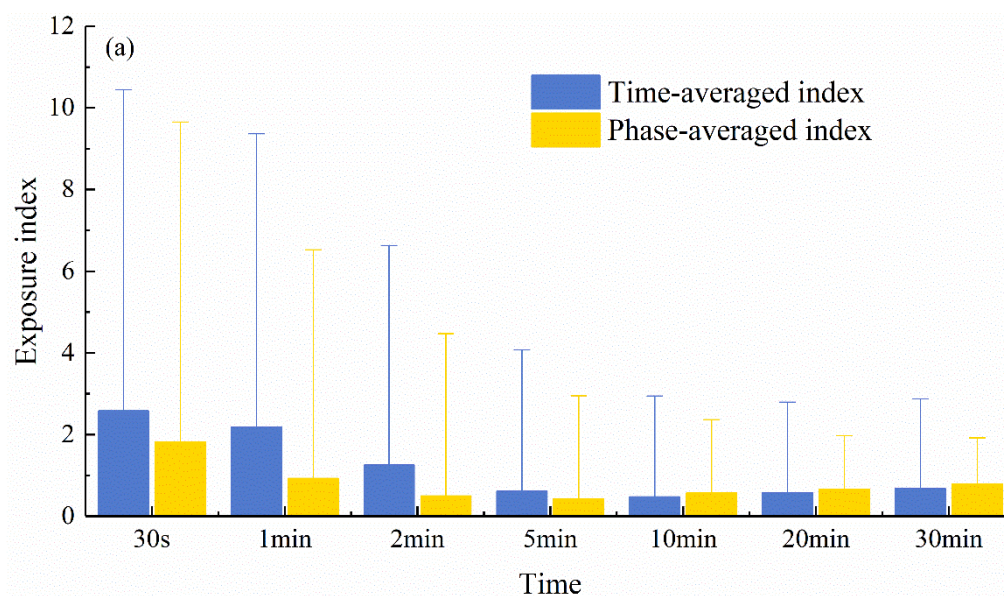
375

## 376 4.2 Comparison of short-term and steady-state exposure

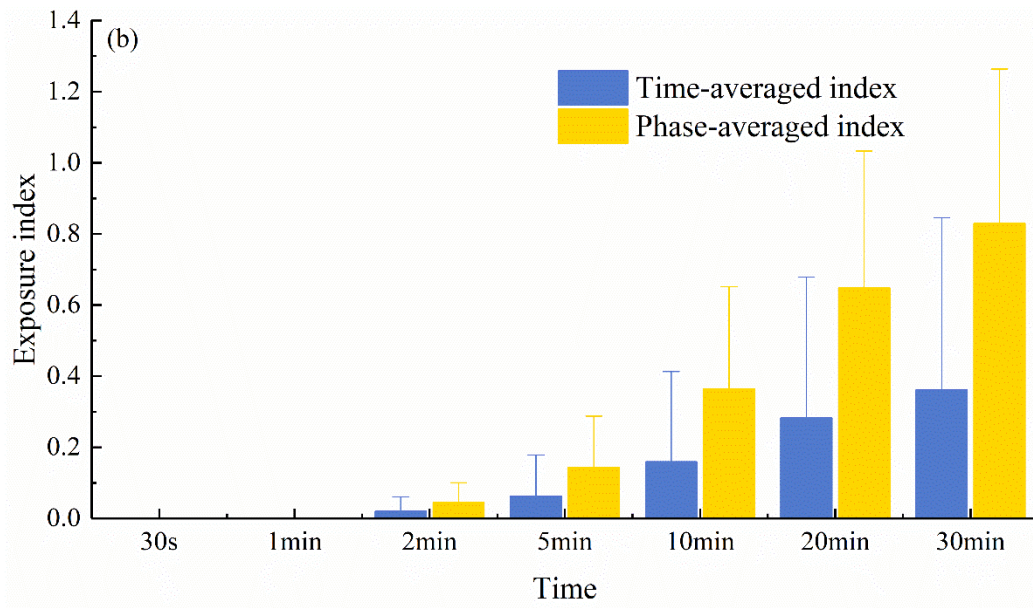
377 As aforementioned, the short-term exposure events could be different depending on the  
 378 status of the indoor background concentration, namely, the steady-state condition and  
 379 the building-up condition [37]. For the building-up condition, the exposure  
 380 characteristics could be distinctive if the exposure duration is different. Fig. 8 presents  
 381 the comparison of the exposure index of various short-term events and steady-state  
 382 event (30 min) based on two exposure indices, namely the time-averaged and phase  
 383 averaged one. Phase-averaged exposure index is calculated only from contaminant  
 384 concentration sampled in the inhalation phase. In comparison, time-averaged exposure  
 385 index is calculated from the arithmetic mean contaminant concentration continuously  
 386 in the exposure event. The error bars refer to the standard deviations of the  
 387 aforementioned two exposure indices. As shown in Fig. 8 (a)(b)(c), the significant

388 standard deviation of exposure indices is found at a separation distance of 0.35 m during  
389 short-term events, which is more moderate at a distance of 1.0 m and 1.5 m. The large  
390 fluctuations demonstrate the randomness and discreteness characteristics of short-term  
391 events (detailed analysis in Section 5). In theory, when the ambient air is completely  
392 mixing under steady-state condition, the exposure index should be unity (1.0). In the  
393 present study, the exposure index slightly deviates from the unity (1.0) due to the  
394 intermittent exhalation of the contaminant and the high-turbulent characteristics of the  
395 flow in the breathing zone.

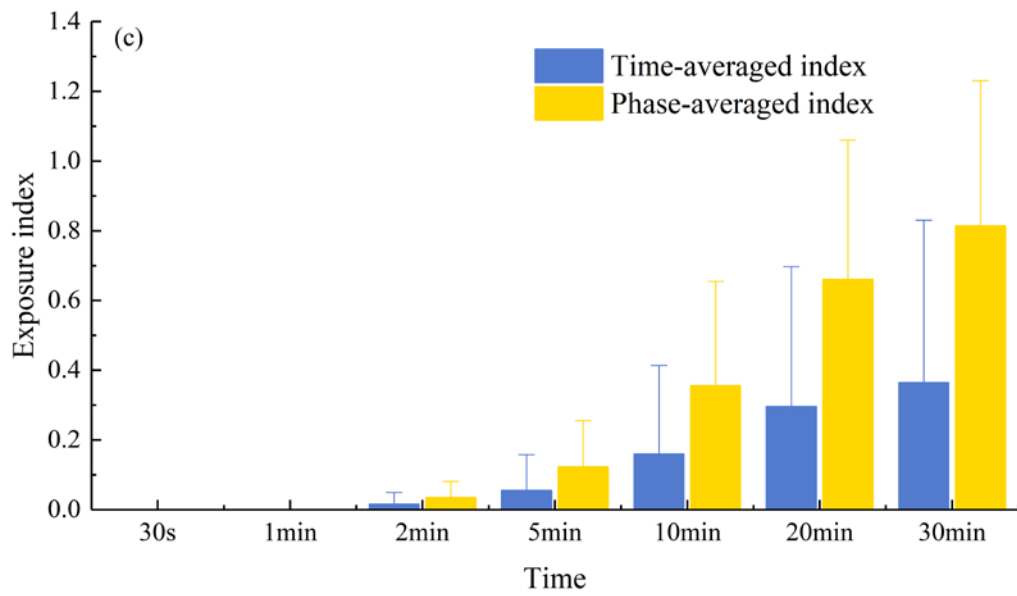
396



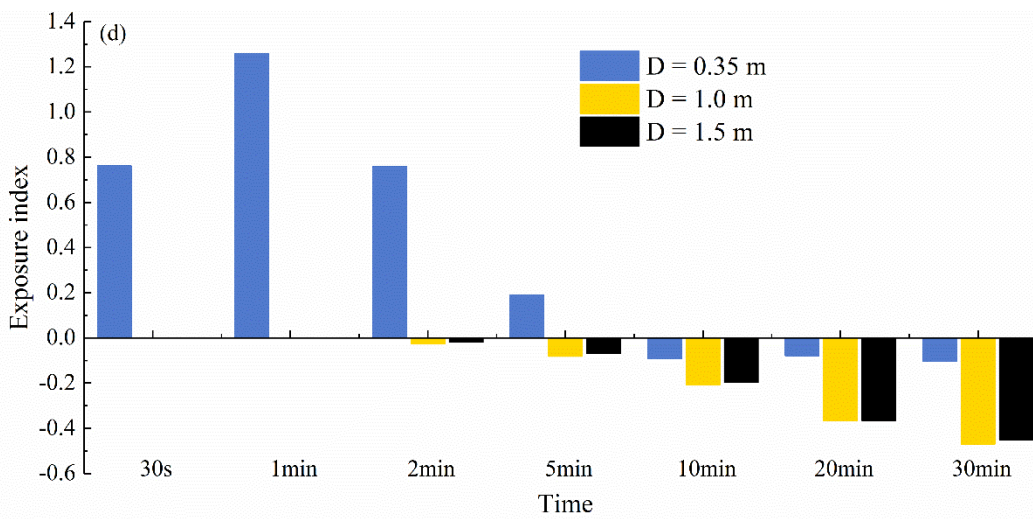
397



398



399



400

401 Fig. 8 Variation of the time-averaged and phase-averaged exposure indices during

402 short-term events under different conditions: a) physical distance of 0.35 m; b) physical  
403 distance of 1.0 m; c) physical distance of 1.5 m; and d) the difference between the time-  
404 averaged and phase-averaged exposure indices.

405

406 In Fig. 8 (a), the physical distance between the two subjects is 0.35 m, and the largest  
407 time-averaged and phase-averaged exposure indices occur in the event duration of 30  
408 s, which are approximately 3 times larger than that under the steady-state condition (30  
409 min). The exposure index does not consistently increase over time, especially before 10  
410 minutes, which agree with previous experimental studies [23]. The high fluctuation  
411 characteristics of the inhaled contaminant concentration could be accounted for by the  
412 strong flow interaction in the breathing zone. The large difference between the time-  
413 averaged and phase-averaged exposure indices is observed at the initial stage, and the  
414 difference becomes smaller with the increase of event duration. The phenomenon is  
415 caused by the absence of phase difference between two breathing cycles, and the high  
416 contaminant concentration presented in the breathing zone of the susceptible subject is  
417 in the exhalation phase (infected subject mouth exhalation and susceptible one nose  
418 exhalation). As shown in Fig. 8 (b) and (c), the time and phase averaged exposure  
419 indices of susceptible subjects at distances of 1.0 m and 1.5 m are generally in the same  
420 trend, and both are obviously lower than that at the distance of 0.35 m. Since the exhaled  
421 pollutants cannot penetrate the thermal convective boundary layer of the susceptible  
422 subject at the distances of 1.0 m and 1.5 m, the time-averaged and phase-averaged  
423 exposure indices are very low in the short-term events within 2 minutes-duration. As

424 the background concentration of contaminants gradually increases, with the increase of  
425 event duration, the exposure index also increases. The difference between the time-  
426 averaged and phase-averaged exposure indices in the long physical distance is owing  
427 to the form of negative pressure zone in the mouth-inhalation phase, allowing the  
428 background contaminant to enter the breathing zone of the susceptible subjects. Fig. 8  
429 (d) refers to the relative difference between the time-averaged and phase-averaged  
430 exposure indices at three physical distances, where the positive value refers to that the  
431 time-averaged exposure index is larger than the phase-averaged one. It indicates the  
432 relative magnitude of the difference of two exposure indices except for their standard  
433 deviations. Due to the clear difference between indices with different trends, both time-  
434 averaged and phase-averaged exposure indices are required to be evaluated in the short-  
435 term events.

436

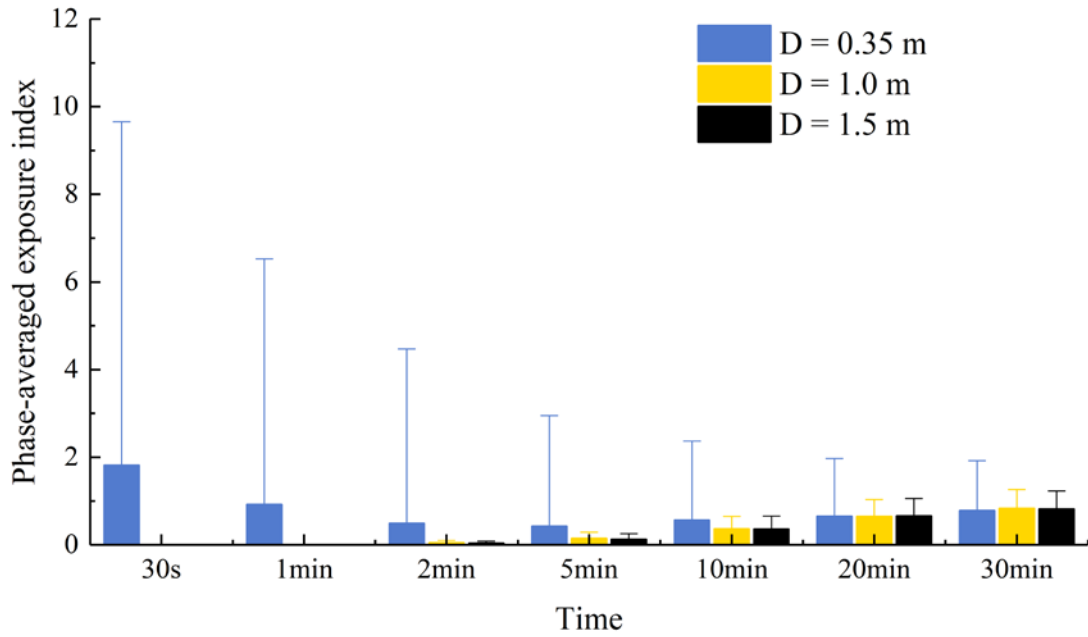
### 437 **4.3 Comparison of exposure index under short and long distances**

438 The relationship between the physical distance and the phase-averaged exposure index  
439 for short-term events with different durations is presented in Fig. 9. Firstly, the physical  
440 distance still acts as a critical parameter for airborne transmission, which refers to the  
441 phase-averaged exposure index generally decreasing as the increase of physical  
442 distance. At a close distance, the exhaled contaminant could directly penetrate the  
443 thermal convective boundary layer of the susceptible subjects. The susceptible subject  
444 is directly exposed to the infected individual. When the physical distance increases to  
445 1.0 m or 1.5 m, the phase-averaged exposure index could decrease. The increasing trend



446 and small fluctuation characteristics at a separation distance of 1.0 m are generally in  
447 line with those of 1.5 m. This may suggest that the indirect transmission dominates the  
448 airborne transmission route, when the physical distance is larger than 1.0 m. Secondly,  
449 the phase-averaged exposure index may not consistently decline as the physical  
450 distance increases. As shown in Fig. 9, the index ( $\varepsilon_{0.35\text{ m}} = 0.651$ ) first slightly  
451 declines ( $\varepsilon_{1.0\text{ m}} = 0.647$ ) and then goes up ( $\varepsilon_{1.5\text{ m}} = 0.659$ ) with the distance for  
452 the exposure period of 20 minutes. The phenomenon could be accounted for by the  
453 instability characteristics of the direct airborne transmission, and it always occurs at a  
454 close physical distance. The detailed assessment of the characteristics of the direct  
455 airborne route would be analyzed in the section 4.4. Thirdly, the phase-averaged  
456 exposure index does not consistently go up over time, particularly for a short physical  
457 distance. Before the 10 min time threshold, the phase-averaged exposure index at 0.35  
458 m slightly decreases over time. After this time threshold, the index slowly increases  
459 over time owing to the increasing background concentration and the occurrence of the  
460 indirect airborne transmission route. It appears that the direct airborne transmission  
461 route plays a more critical role than the indirect one at a short separation distance during  
462 short-term events. Owing to the presence of direct and indirect airborne transmission in  
463 the short separation distance, the change of the room ventilation rate could affect the  
464 time threshold and the occurrence time of the indirect airborne route. In order to further  
465 understand the mechanism of airborne transmission, it is important to separate the direct  
466 and indirect airborne transmission routes.

467



468

469 Fig. 9 The relationship between the physical distance and the phase-averaged

470 exposure index in short-term events with different durations

471

#### 472 4.4 Separation of the airborne transmission routes

473 Notably, the employed time-averaged and phase-averaged exposure index (as presented

474 in Fig. 8 and 9) just indicate the average contaminant concentration inhaled by the

475 susceptible subject, but do not reveal the cumulation of inhaled contaminant over time.

476 Fig. 10 presents the cumulative exposure index at different physical distances. The

477 cumulative exposure index continues to grow over time, and the physical distance still

478 acts as the dominant role in the exposure assessment. Differences are found in the

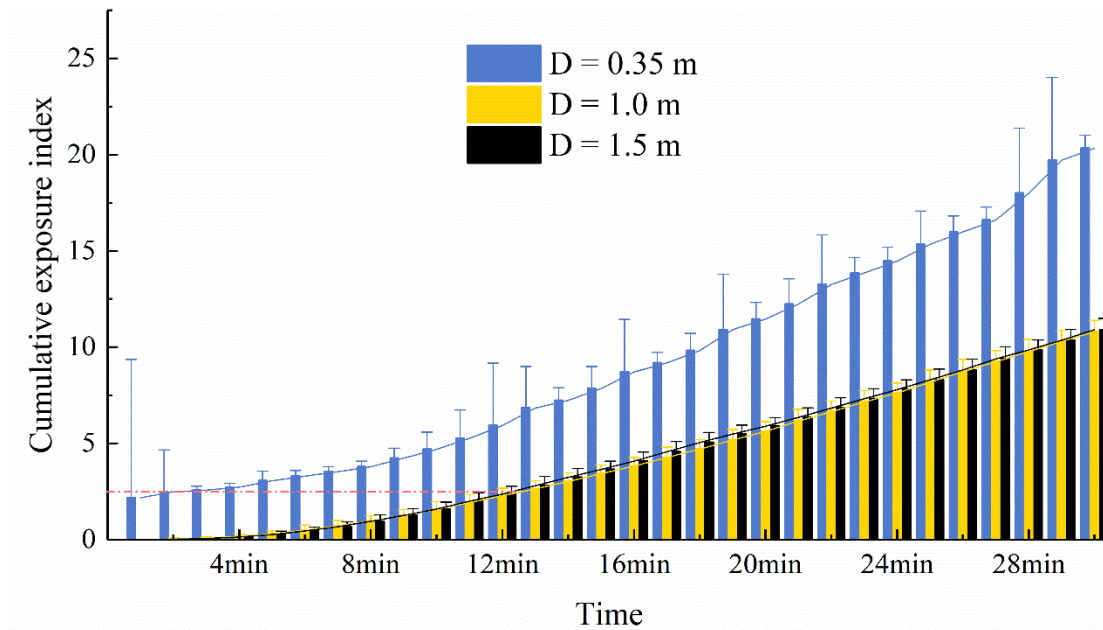
479 growth rate of the exposure index between the scenarios at different physical distances

480 and with different exposure durations. The exposure risk in a 2-minute exposure event

481 at the distance of 0.35 m is approximately equal to that in the 12-minute exposure

482 scenario at 1.5 m/1.0 m. In addition, at the distance of 0.35 m, the difference between

483 the slopes before and after 10 min may be due to the change in the relative role of the  
484 two airborne transmission routes, namely direct or indirect transmission. The insight of  
485 the characteristics of airborne transmission could help to develop accurate mitigation  
486 measures.



487

488 Fig. 10 The cumulative time-averaged exposure index at different physical distances  
489 with the interval of 1 min

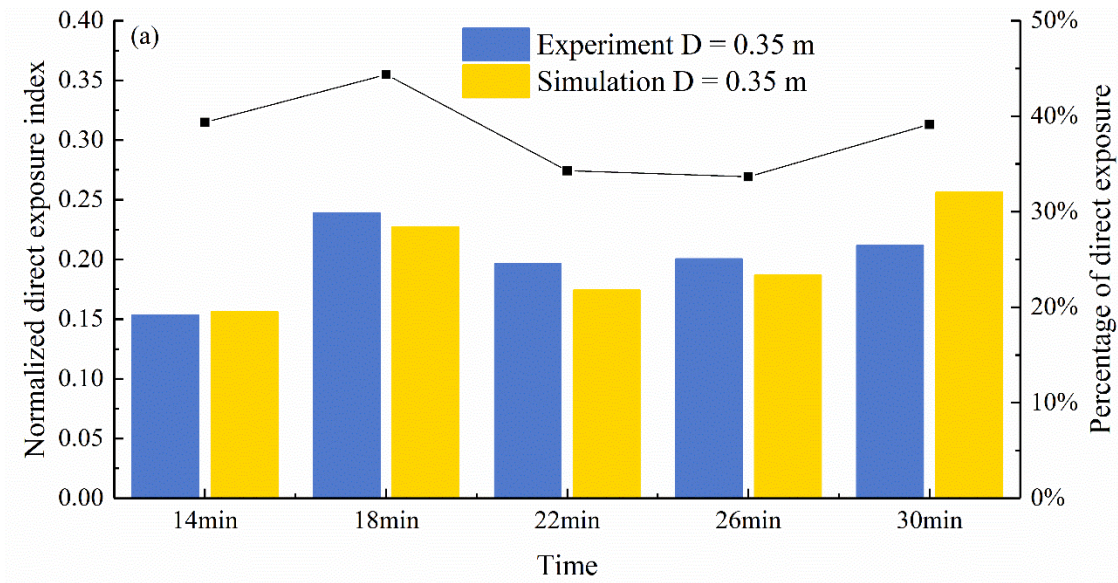
490

491 According to the occurrence time of the indirect airborne transmission route in this  
492 study, it is assumed that indirect exposure could increase uniformly after 10 minutes.

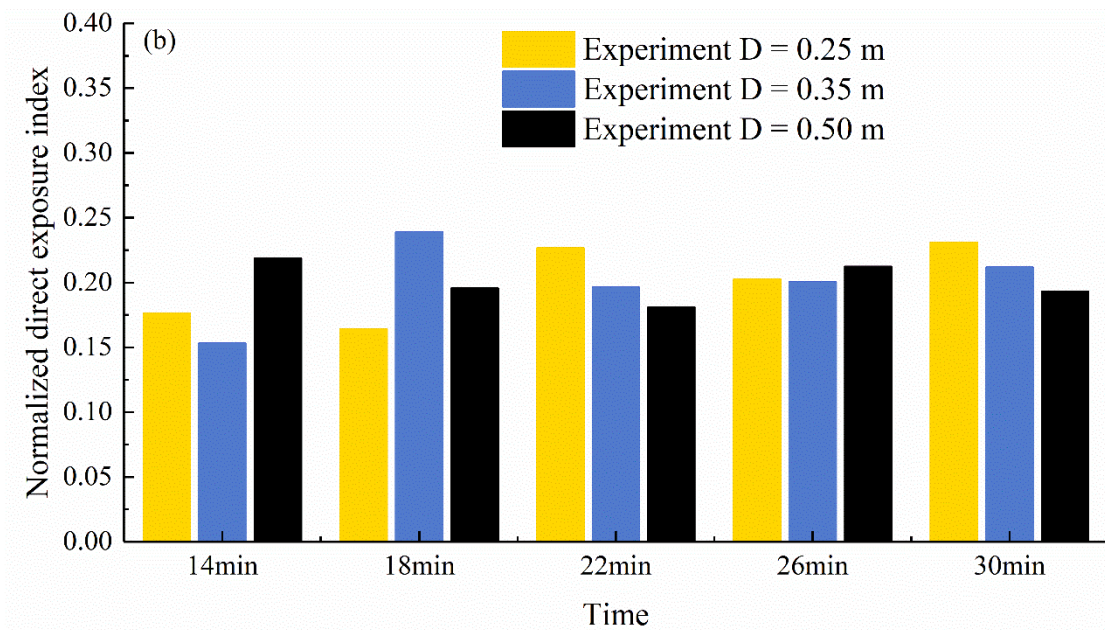
493 As mentioned above, the two airborne transmission routes occur when the susceptible  
494 subject is in close proximity to the infected one (at 0.35 m), and only the indirect route  
495 exists at large physical distances (at 1.0 m/1.5 m). In this way, the direct exposure of  
496 airborne transmission at a distance of 0.35 m can be calculated by subtracting the  
497 exposure at 1.5 m (representing indirect exposure) from the exposure at 0.35 m

498 (representing total exposure). The results of experiments performed in the large-space  
499 university canteen (see section 3.1 for details) are also used for comparison. As  
500 presented in Fig. 11, the direct exposure indices at different physical distances are  
501 compared through the normalization  $\overline{\varepsilon_i(m)}/\sum \overline{\varepsilon_i(m)}$  where the  $\overline{\varepsilon_i(m)}$  refers to the  
502 direct exposure indices for the interval of time  $m$ . In Fig. 11 (a), the direct exposure  
503 indices obtained by simulation and experiment have presented the same instability  
504 characteristics. In comparison with the indirect exposure index stably increasing with  
505 time, the direct exposure index could fluctuate over time. The instability might be  
506 accounted for by the presence of turbulence, rising from the strong flow interaction in  
507 breathing zone. In addition, the percentage of direct exposure to total exposure could  
508 also change largely over time, and it fluctuates around 40% after 10 minutes. Note that  
509 this percentage should be strongly influenced by the air change rate of the space. Fig.  
510 11 (b) presents the direct exposure indices in the supplementary experiment study with  
511 three close physical distances (0.25 m, 0.35 m, and 0.5 m). Since the background  
512 concentration (referring to indirect exposure) in the large experimental space is  
513 negligible, the averaged direct exposure indices obtained in the three close distances  
514 would be presented as generally similar. Nevertheless, the discreteness of the exposure  
515 index generally decreases with increasing physical distance. Considering the  
516 randomness, discreteness, localization, and high-risk characteristics of direct airborne  
517 transmission route, current precautionary actions and the dilution ventilation aiming for  
518 the whole space under steady-state condition could not be high-efficient for the short-  
519 term events.

520



521



522

523 Fig. 11 Comparison about the normalized direct exposure indices at different physical

524 distances: a) the results obtained by simulation and experiment at a distance of 0.35

525 m; b) the direct exposure indices at three close distances

526

## 527 5. Discussion

528 Depending on the exposure duration and separation distance, airborne transmission

529 could be divided into two categories and four combinations, namely, a) steady-state  
530 exposure: short-distance and long-distance; b) short-term exposure: short-distance and  
531 long-distance. Many previous studies focused on steady-state exposure [10, 11, 53], but  
532 fewer studied the short-term exposure events. In real life, there are many short-term  
533 exposure events, such as the consultation of physicians, short meetings, offices,  
534 classrooms, canteens, etc. In response to the Delta and Omicron variants of SARS-CoV-  
535 2, the airborne transmission in the short-term events should be well recognized by the  
536 public health authorities. Maintaining physical distance and wearing masks continue to  
537 be effective mitigation strategies for the Delta and Omicron variants [54, 55]. To  
538 maintain the health and well-being of urban dwellers [56], the physical distancing is  
539 still recommended for short-term events.

540

541 In contrary to the previous study [57], the result of this study illustrates that the  
542 exposure index for the short-term exposure events might not consistently increase over  
543 time until reaching the steady-state condition. During the short-term events with a short  
544 physical distance (0.35 m), the largest time-averaged exposure index is presented in the  
545 short-term events with the duration of 30 s, where the exposure index is around 3 times  
546 higher than that of the steady-state condition. As mentioned early, the short-term events  
547 investigated in the present study is restricted to the scenarios with building-up  
548 background concentration. The strong interaction of flows in the breathing zone could  
549 result in the inhaled concentration being unstable and changing over time [23]. The  
550 magnitude of concentration fluctuation also affects the exposure in short-term events.

551 Therefore, the time or phase averaged exposure index might be smaller in the steady-  
552 state condition (as an example shown in Fig. 8). The obtained result also explains that  
553 the reported infection of the Delta variant of SARS-CoV-2 may occur in tens of seconds  
554 [6]. In addition, the exposure index investigated in this study for various short-term  
555 events might not consistently decline as the physical distances increase (as presented in  
556 Fig. 9), the obtained results are not consistent with the observation under steady-state  
557 conditions [58, 59]. Because of the random fluctuation of the direct airborne  
558 transmission route during short-term events, the higher value of the time-averaged  
559 exposure index could occur in the relatively long physical distance. In general, the  
560 difference between the short-term events and the steady-state condition implies that the  
561 current mitigation methods and the dilution ventilation based on the steady-state  
562 condition might not be high-efficient for the short-term events. The development of  
563 effective precautionary measures aiming for short-term or unsteady exposures events is  
564 expected to receive much more attention.

565

566 The large fluctuation characteristics of the short-term exposure index are observed, no  
567 matter in the short and the long physical distance. Owing to the instantaneous and tidal  
568 characteristics of the exhalation jet, it becomes fully turbulent and further mixes with  
569 the surrounding air with the development of flow. In addition, the interaction between  
570 respiratory flow, the ventilation flow, and the thermal convective boundary layer rising  
571 from the heated human body increases the turbulence level in the breathing zone of  
572 susceptible subjects. For example, at the physical distance of 0.35 m, the high

573 fluctuation of the concentration of contaminants inhaled by the susceptible subjects can  
574 be explained by the strong interaction between the flow of two exhalations. The  
575 interaction may cause the inhomogeneous distribution of concentration in the breathing  
576 zone. Therefore, it is absolutely necessary to distinguish the difference between  
577 concentration distribution in the breathing zone and that inhaled by the susceptible  
578 subject. At the long physical distance like 1.0 m and 1.5 m, the relative lower fluctuation  
579 of the concentration is due to the mixing and dilution effect of the surrounding flow.

580

581 The infection risk assessment could act as an effective tool to evaluate the exposure risk  
582 of susceptible subjects and validate the performance of the corresponding precautionary  
583 measures. In this study, an improved evaluation method proposed by Ai et al. [23] is  
584 employed to evaluate the airborne transmission risk under the short-term events. The  
585 traditionally widely used risk-evaluation methods such as the Wells-Riley equations, IF  
586 (intake fraction), and exposure index have presented their limitations with regard to the  
587 unsteady and short-term exposure events. Considering that there are many short-term  
588 events in practice and that even the steady-state and complete-mixing are not reached  
589 before the end of the events, the improved evaluation method makes it possible to  
590 evaluate both real-time exposure risk of the susceptible subject at one particular  
591 moment and time-averaged exposure risk over a given period.

592

593 Increasing the room ventilation rate is a widely recommended measure to dilute the  
594 concentration and further control the airborne transmission. However, the direct



595 airborne transmission occurs with the direct exposure of the virus-laden droplets and  
596 aerosols when the subjects are in close physical proximity. The results of the present  
597 study illustrate that direct airborne transmission is much more important than indirect  
598 one in short-term events. This is because the room ventilation could dilute and reduce  
599 the background concentration, but the background value in the short-term events is  
600 relatively lower and not uniform than that in the steady state. Therefore, the general  
601 dilution ventilation has a limited impact on the direct airborne transmission in short-  
602 term events. In addition, the separation of the airborne routes and the further assessment  
603 of their associated properties have proven the previous hypothesis that the SARS-CoV-  
604 2 transmission is predominated by the direct airborne route [60]. Compared to the  
605 limited impact on the direct airborne route, the general dilution ventilation could  
606 determine the occurrence time of indirect one. The relationship between different room  
607 ventilation rates and the occurrence time of indirect airborne route needs further  
608 assessment. Owing to the randomness, discreteness, localization, and high-risk  
609 characteristics of the direct airborne route, the current precautionary actions and the  
610 dilution ventilation based on the whole space under steady-state condition could not be  
611 high-efficient for the short-term events. The localized ventilation/exhaust system, air  
612 curtain, physical barrier, and air filtration should be highly recommended. From the  
613 perspective of engineering control, protection measures can be divided into two types,  
614 namely, control of the emission from the infected and protection of the susceptible. The  
615 widely recommended surgical mask may help to filter most of droplets and also  
616 extinguish the exhalation jet. A physical barrier would also be effective to block the

617 exhalation jet [61]. For places with a high requirement, the escaping fine particles could  
618 be further removed by a localized exhaust system.

619

620 As for the limitation of this study, the exhaled contaminant is surrogated by the tracer  
621 gas. The discrete phase with evaporation process is not considered for several reasons:  
622 Firstly, the size distribution of the respiratory droplet and aerosol particles are found in  
623 the range from 0.25 to 40  $\mu\text{m}$ , and the most fall into the 1-4  $\mu\text{m}$  [45]. Given that the  
624 main driving force for the respiratory particles in the indoor environment is the airflow  
625 rather than the gravity [62], the tracer gas is suitable to simulate this commonest range  
626 of respiratory particles [45]. Secondly, the evaporation process is instantaneous for  
627 small droplets [63]. A 3 and 5  $\mu\text{m}$  pure-water droplet would evaporate at 97% relative  
628 humidity in less than 0.33 s and 0.8 s, respectively [64]. Therefore, the present study  
629 employs the tracer gas rather than the discrete phases with evaporation to simulate the  
630 transmission of the respiratory particles. Future study should examine the transmission  
631 pattern of the large droplets. In addition, the study is limited to the condition where  
632 human is still, while the movement of the body significantly affects the convective  
633 boundary layer and further influences the cross-transmission [65]. The present study  
634 does not consider the droplet route and surface contact route, which, however,  
635 contribute a lot to the overall risk of cross infection. Finally, it should be noted that the  
636 study only focuses on the scenario of building-up background concentration at a certain  
637 air change rate (namely, 6  $\text{h}^{-1}$ ).

638

639 **6. Conclusions**

640 The present study on direct and indirect airborne transmission during short-term events  
641 allows the following conclusions to be drawn:

642 1) The exposure index in the short-term events varies largely over time, especially  
643 within the first 1/ACH hour (namely, 10 minutes in the present study) of exposure  
644 between occupants in close proximity. Due to such a considerable variation, there  
645 is a high uncertainty related to the spatial and temporal evolutions of the risk of  
646 cross infection.

647 2) The decoupling and analysis of the direct and indirect airborne transmission routes  
648 have shown that the direct airborne transmission acts as the predominated route in  
649 short-term events. The conventional dilution ventilation has a limited influence on  
650 the direct airborne transmission route, but, to a large extent, determines the  
651 occurrence time of indirect one.

652 3) Owing to the randomness, discreteness, localization, and high-risk characteristics  
653 of direct airborne transmission, the current precautionary measures aiming for the  
654 whole space under steady-state conditions are not high-efficient to the short-term  
655 events, and localized methods like localized ventilation/exhaust system and  
656 physical barrier that can effectively destroy the direct airborne transmission route  
657 should be more effective and less costly.

658

659 **Acknowledgements**

660 This study was supported by the National Natural Science Foundation of China (No.

661 51908203) and by the Fundamental Research Funds for the Central Universities (No.  
662 531118010378). The authors thank Miss Zenan Xian for her help in the pre - project  
663 work.

664

### 665 **Author Contribution**

666 All authors contributed to the study conception and design. Material preparation, data  
667 collection and analysis were performed by Xiujie Li, Zhengtao Ai, and Jinjun Ye. The  
668 first draft of the manuscript was written by Xiujie Li, and Zhengtao Ai. All authors  
669 commented on previous versions of the manuscript. All authors read and approved the  
670 final manuscript.

671

### 672 **Declaration of competing interest**

673 The authors declare that they have no known competing financial interests or personal  
674 relationships that could have appeared to influence the work reported in this paper.

675

### 676 **Reference**

- 677 [1] WHO, "Weekly epidemiological update on COVID-19 - 12 April ", 2022. [Online]. Available:  
678 [https://www.who.int/publications/m/item/weekly-epidemiological-update-on-covid-19---12-](https://www.who.int/publications/m/item/weekly-epidemiological-update-on-covid-19---12-april-2022)  
679 [april-2022](https://www.who.int/publications/m/item/weekly-epidemiological-update-on-covid-19---12-april-2022)
- 680 [2] Y. Liu *et al.*, "Aerodynamic analysis of SARS-CoV-2 in two Wuhan hospitals," *Nature*, vol. 582,  
681 no. 7813, pp. 557-560, 2020.
- 682 [3] X. Li, C. M. Mak, K. W. Ma, and H. M. Wong, "Restoration of dental services after COVID-19:  
683 The fallow time determination with laser light scattering," *Sustainable Cities and Society*, vol.  
684 74, p. 103134, 2021.
- 685 [4] X. Li, C. M. Mak, K. W. Ma, and H. M. Wong, "Evaluating flow-field and expelled droplets in  
686 the mockup dental clinic during the COVID-19 pandemic," *Physics of Fluids*, vol. 33, no. 4, p.  
687 047111, 2021.
- 688 [5] N. Van Doremalen *et al.*, "Aerosol and surface stability of SARS-CoV-2 as compared with

- 689 SARS-CoV-1," *New England journal of medicine*, vol. 382, no. 16, pp. 1564-1567, 2020.
- 690 [6] T. Kongnov. "Delta can spread in 15 seconds." <https://www.khmertimeskh.com/50902050/delta-can-spread-in-15-seconds/> (accessed.
- 691
- 692 [7] K. Times. "Delta variant can infect a person within 15 seconds as Cambodia logs 75 total cases
- 693 of COVID-19 Delta infections." [https://www.khmertimeskh.com/50895595/delta-variant-can-](https://www.khmertimeskh.com/50895595/delta-variant-can-infect-a-person-within-15-seconds-as-cambodia-logs-75-cases-of-covid-19-delta-infections/)
- 694 [infect-a-person-within-15-seconds-as-cambodia-logs-75-cases-of-covid-19-delta-infections/](https://www.khmertimeskh.com/50895595/delta-variant-can-infect-a-person-within-15-seconds-as-cambodia-logs-75-cases-of-covid-19-delta-infections/)
- 695 (accessed.
- 696 [8] M. K. Satheesan, K. W. Mui, and L. T. Wong, "A numerical study of ventilation strategies for
- 697 infection risk mitigation in general inpatient wards," in *Building simulation*, 2020, vol. 13, no.
- 698 4: Springer, pp. 887-896.
- 699 [9] N. Massarotti, A. Mauro, S. Mohamed, A. J. Nowak, and D. Sainas, "Fluid dynamic and
- 700 thermal comfort analysis in an actual operating room with unidirectional airflow system," in
- 701 *Building Simulation*, 2021, vol. 14, no. 4: Springer, pp. 1127-1146.
- 702 [10] S. Srivastava, X. Zhao, A. Manay, and Q. Chen, "Effective ventilation and air disinfection
- 703 system for reducing Coronavirus Disease 2019 (COVID-19) infection risk in office buildings,"
- 704 *Sustainable Cities and Society*, vol. 75, p. 103408, 2021.
- 705 [11] H. Motamedi, M. Shirzadi, Y. Tominaga, and P. A. Mirzaei, "CFD modeling of airborne
- 706 pathogen transmission of COVID-19 in confined spaces under different ventilation strategies,"
- 707 *Sustainable Cities and Society*, vol. 76, p. 103397, 2022.
- 708 [12] H. Wang, H. Qian, R. Zhou, and X. Zheng, "A novel circulated air curtain system to confine
- 709 the transmission of exhaled contaminants: A numerical and experimental investigation," in
- 710 *Building Simulation*, 2020, vol. 13, no. 6: Springer, pp. 1425-1437.
- 711 [13] Z. Zhang, T. Han, K. H. Yoo, J. Capecehatro, A. L. Boehman, and K. Maki, "Disease
- 712 transmission through expiratory aerosols on an urban bus," *Physics of Fluids*, vol. 33, no. 1, p.
- 713 015116, 2021.
- 714 [14] L. Zhao, H. Zhou, Y. Jin, and Z. Li, "Experimental and numerical investigation of TVOC
- 715 concentrations and ventilation dilution in enclosed train cabin," in *Building Simulation*, 2022,
- 716 vol. 15, no. 5: Springer, pp. 831-844.
- 717 [15] P. Armand and J. Tâche, "3D modelling and simulation of the dispersion of droplets and drops
- 718 carrying the SARS-CoV-2 virus in a railway transport coach," *Scientific Reports*, vol. 12, no. 1,
- 719 pp. 1-22, 2022.
- 720 [16] D. Bhatia and A. De Santis, "A preliminary numerical investigation of airborne droplet
- 721 dispersion in aircraft cabins," *Open Journal of Fluid Dynamics*, vol. 10, no. 3, pp. 198-207,
- 722 2020.
- 723 [17] P. S. Desai, N. Sawant, and A. Keene, "On COVID-19-safety ranking of seats in
- 724 intercontinental commercial aircrafts: A preliminary multiphysics computational perspective,"
- 725 in *Building simulation*, 2021, vol. 14, no. 6: Springer, pp. 1585-1596.
- 726 [18] J. Villafruela, I. Olmedo, and J. San José, "Influence of human breathing modes on airborne
- 727 cross infection risk," *Building and Environment*, vol. 106, pp. 340-351, 2016.
- 728 [19] C. Yang, X. Yang, and B. Zhao, "Person to person droplets transmission characteristics in
- 729 unidirectional ventilated protective isolation room: The impact of initial droplet size," in
- 730 *Building Simulation*, 2016, vol. 9, no. 5: Springer, pp. 597-606.
- 731 [20] J. Wu and W. Weng, "COVID-19 virus released from larynx might cause a higher exposure dose
- 732 in indoor environment," *Environmental Research*, vol. 199, p. 111361, 2021.

- 733 [21] Z. T. Ai and A. K. Melikov, "Airborne spread of expiratory droplet nuclei between the occupants  
734 of indoor environments: A review," *Indoor air*, vol. 28, no. 4, pp. 500-524, 2018.
- 735 [22] E. Riley, G. Murphy, and R. Riley, "Airborne spread of measles in a suburban elementary  
736 school," *American journal of epidemiology*, vol. 107, no. 5, pp. 421-432, 1978.
- 737 [23] Z. Ai, K. Hashimoto, and A. K. Melikov, "Airborne transmission between room occupants  
738 during short-term events: Measurement and evaluation," *Indoor air*, vol. 29, no. 4, pp. 563-576,  
739 2019.
- 740 [24] Z. Ai, C. M. Mak, and J. Niu, "Numerical investigation of wind-induced airflow and interunit  
741 dispersion characteristics in multistory residential buildings," *Indoor air*, vol. 23, no. 5, pp. 417-  
742 429, 2013.
- 743 [25] Z. Ai and C. M. Mak, "A study of interunit dispersion around multistory buildings with single-  
744 sided ventilation under different wind directions," *Atmospheric Environment*, vol. 88, pp. 1-13,  
745 2014.
- 746 [26] Y. Dai, C. M. Mak, and Z. Ai, "Computational fluid dynamics simulation of wind-driven inter-  
747 unit dispersion around multi-storey buildings: Upstream building effect," *Indoor and Built  
748 Environment*, vol. 28, no. 2, pp. 217-234, 2019.
- 749 [27] Y. Dai, C. M. Mak, Z. Ai, and J. Hang, "Evaluation of computational and physical parameters  
750 influencing CFD simulations of pollutant dispersion in building arrays," *Building and  
751 Environment*, vol. 137, pp. 90-107, 2018.
- 752 [28] A. K. Melikov, Z. Ai, and D. Markov, "Intermittent occupancy combined with ventilation: An  
753 efficient strategy for the reduction of airborne transmission indoors," *Science of The Total  
754 Environment*, vol. 744, p. 140908, 2020.
- 755 [29] X. Li, C. M. Mak, K. W. Ma, and H. M. Wong, "How the high-volume evacuation alters the  
756 flow-field and particle removal characteristics in the mock-up dental clinic," *Building and  
757 Environment*, vol. 205, p. 108225, 2021.
- 758 [30] J. Hinze, "Secondary currents in wall turbulence," *The Physics of Fluids*, vol. 10, no. 9, pp.  
759 S122-S125, 1967.
- 760 [31] J. Smagorinsky, "General circulation experiments with the primitive equations: I. The basic  
761 experiment," *Monthly weather review*, vol. 91, no. 3, pp. 99-164, 1963.
- 762 [32] Z. Ai and C. M. Mak, "Large-eddy Simulation of flow and dispersion around an isolated  
763 building: analysis of influencing factors," *Computers & Fluids*, vol. 118, pp. 89-100, 2015.
- 764 [33] Y. Du, B. Blocken, S. Abbasi, and S. Pirker, "Efficient and high-resolution simulation of  
765 pollutant dispersion in complex urban environments by island-based recurrence CFD,"  
766 *Environmental Modelling & Software*, vol. 145, p. 105172, 2021.
- 767 [34] W. Liu *et al.*, "Exploring the potentials of personalized ventilation in mitigating airborne  
768 infection risk for two closely ranged occupants with different risk assessment models," *Energy  
769 and Buildings*, vol. 253, p. 111531, 2021.
- 770 [35] A. K. Melikov and V. Dzhartov, "Advanced air distribution for minimizing airborne cross-  
771 infection in aircraft cabins," *Hvac&R Research*, vol. 19, no. 8, pp. 926-933, 2013.
- 772 [36] N. Gao and J. Niu, "Modeling particle dispersion and deposition in indoor environments,"  
773 *Atmospheric environment*, vol. 41, no. 18, pp. 3862-3876, 2007.
- 774 [37] Z. Ai, T. Huang, and A. Melikov, "Airborne transmission of exhaled droplet nuclei between  
775 occupants in a room with horizontal air distribution," *Building and Environment*, vol. 163, p.  
776 106328, 2019.

- 777 [38] Z. Ai, K. Hashimoto, and A. K. Melikov, "Influence of pulmonary ventilation rate and breathing  
778 cycle period on the risk of cross-infection," *Indoor air*, vol. 29, no. 6, pp. 993-1004, 2019.
- 779 [39] N. Zaproudina, V. Varmavuo, O. Airaksinen, and M. Närhi, "Reproducibility of infrared  
780 thermography measurements in healthy individuals," *Physiological measurement*, vol. 29, no.  
781 4, p. 515, 2008.
- 782 [40] D. Licina, J. Pantelic, A. Melikov, C. Sekhar, and K. W. Tham, "Experimental investigation of  
783 the human convective boundary layer in a quiescent indoor environment," *Building and  
784 Environment*, vol. 75, pp. 79-91, 2014.
- 785 [41] A. Melikov, "Breathing thermal manikins for indoor environment assessment: important  
786 characteristics and requirements," *European journal of applied physiology*, vol. 92, no. 6, pp.  
787 710-713, 2004.
- 788 [42] C. Xu, P. V. Nielsen, L. Liu, R. L. Jensen, and G. Gong, "Human exhalation characterization  
789 with the aid of schlieren imaging technique," *Building and environment*, vol. 112, pp. 190-199,  
790 2017.
- 791 [43] Z. D. Bolashikov, M. Barova, and A. K. Melikov, "Wearable personal exhaust ventilation:  
792 Improved indoor air quality and reduced exposure to air exhaled from a sick doctor," *Science  
793 and Technology for the Built Environment*, vol. 21, no. 8, pp. 1117-1125, 2015.
- 794 [44] J. Yang, C. Sekhar, D. K. Cheong, and B. Raphael, "A time-based analysis of the personalized  
795 exhaust system for airborne infection control in healthcare settings," *Science and Technology  
796 for the Built Environment*, vol. 21, no. 2, pp. 172-178, 2015.
- 797 [45] Z. Ai, C. M. Mak, N. Gao, and J. Niu, "Tracer gas is a suitable surrogate of exhaled droplet  
798 nuclei for studying airborne transmission in the built environment," in *Building Simulation*,  
799 2020, vol. 13, no. 3: Springer, pp. 489-496.
- 800 [46] J. Villafruela, I. Olmedo, M. R. De Adana, C. Méndez, and P. V. Nielsen, "CFD analysis of the  
801 human exhalation flow using different boundary conditions and ventilation strategies," *Building  
802 and Environment*, vol. 62, pp. 191-200, 2013.
- 803 [47] A. Fluent, "ANSYS Fluent 12.0 user's guide," *Ansys Inc*, vol. 15317, pp. 1-2498, 2009.
- 804 [48] F. Arpino, G. Cortellessa, G. Grossi, and H. Nagano, "A Eulerian-Lagrangian approach for the  
805 non-isothermal and transient CFD analysis of the aerosol airborne dispersion in a car cabin,"  
806 *Building and Environment*, vol. 209, p. 108648, 2022.
- 807 [49] L. Liu, Y. Li, P. V. Nielsen, J. Wei, and R. L. Jensen, "Short-range airborne transmission of  
808 expiratory droplets between two people," *Indoor air*, vol. 27, no. 2, pp. 452-462, 2017.
- 809 [50] F. Liu, C. Zhang, H. Qian, X. Zheng, and P. V. Nielsen, "Direct or indirect exposure of exhaled  
810 contaminants in stratified environments using an integral model of an expiratory jet," *Indoor  
811 air*, vol. 29, no. 4, pp. 591-603, 2019.
- 812 [51] L. Feng, S. Yao, H. Sun, N. Jiang, and J. Liu, "TR-PIV measurement of exhaled flow using a  
813 breathing thermal manikin," *Building and environment*, vol. 94, pp. 683-693, 2015.
- 814 [52] G. Feng, Y. Bi, Y. Zhang, Y. Cai, and K. Huang, "Study on the motion law of aerosols produced  
815 by human respiration under the action of thermal plume of different intensities," *Sustainable  
816 cities and society*, vol. 54, p. 101935, 2020.
- 817 [53] S. Bhattacharyya, K. Dey, A. R. Paul, and R. Biswas, "A novel CFD analysis to minimize the  
818 spread of COVID-19 virus in hospital isolation room," *Chaos, Solitons & Fractals*, vol. 139, p.  
819 110294, 2020.
- 820 [54] S. Leonard *et al.*, "Reducing aerosol dispersion by high flow therapy in COVID-19: High

821 resolution computational fluid dynamics simulations of particle behavior during high velocity  
822 nasal insufflation with a simple surgical mask," *Journal of the American College of Emergency*  
823 *Physicians Open*, vol. 1, no. 4, pp. 578-591, 2020.

824 [55] A. Khosronejad *et al.*, "Fluid dynamics simulations show that facial masks can suppress the  
825 spread of COVID-19 in indoor environments," *Aip Advances*, vol. 10, no. 12, p. 125109, 2020.

826 [56] X. Li, Y. Wei, J. Zhang, and P. Jin, "Design and analysis of an active daylight harvesting system  
827 for building," *Renewable Energy*, vol. 139, pp. 670-678, 2019.

828 [57] M. Buus, F. Winther, and M. Thilageswaran, "Contaminant flow in the microenvironment  
829 between people under different ventilation conditions," *Ashrae Transactions*, vol. 114, p. 632,  
830 2008.

831 [58] Z. D. Bolashikov, A. K. Melikov, W. Kierat, Z. Popiołek, and M. Brand, "Exposure of health  
832 care workers and occupants to coughed airborne pathogens in a double-bed hospital patient  
833 room with overhead mixing ventilation," *Hvac&R Research*, vol. 18, no. 4, pp. 602-615, 2012.

834 [59] I. Olmedo, P. V. Nielsen, M. Ruiz de Adana, and R. L. Jensen, "The risk of airborne cross-  
835 infection in a room with vertical low-velocity ventilation," *Indoor Air*, vol. 23, no. 1, pp. 62-73,  
836 2013.

837 [60] Y. Li, "Hypothesis: SARS-CoV-2 transmission is predominated by the short-range airborne  
838 route and exacerbated by poor ventilation," *Indoor Air*, vol. 31, no. 4, p. 921, 2021.

839 [61] J. Ye, Z. Ai, and C. Zhang, "A new possible route of airborne transmission caused by the use of  
840 a physical partition," *Journal of Building Engineering*, vol. 44, p. 103420, 2021.

841 [62] W. W. Nazaroff, "Indoor bioaerosol dynamics," *Indoor Air*, vol. 26, no. 1, pp. 61-78, 2016.

842 [63] H. Holmgren, B. Bake, A.-C. Olin, and E. Ljungström, "Relation between humidity and size of  
843 exhaled particles," *Journal of aerosol medicine and pulmonary drug delivery*, vol. 24, no. 5, pp.  
844 253-260, 2011.

845 [64] L. Morawska *et al.*, "Size distribution and sites of origin of droplets expelled from the human  
846 respiratory tract during expiratory activities," *Journal of aerosol science*, vol. 40, no. 3, pp. 256-  
847 269, 2009.

848 [65] S.-J. Cao, D. Cen, W. Zhang, and Z. Feng, "Study on the impacts of human walking on indoor  
849 particles dispersion using momentum theory method," *Building and Environment*, vol. 126, pp.  
850 195-206, 2017.

851